Ann. Telecommun. (2013) 68:49–55
DOI 10.1007/s12243-012-0351-6

90° SOI optical hybrid for Radio-over-fibre links

Sawsan Abdul-Majid · Imad Hasan · Qi Zheng · Ramón Maldonado-Basilio · Serge Bidnyk · Trevor Hall

Received: 29 November 2011 / Accepted: 20 November 2012 / Published online: 13 January 2013

Abstract Radio-over- fibre (RoF) technology is receiving large attention due to its ability to provide simple antenna front ends, increased capacity and increased wireless access coverage. Coherently detected RoF systems would enable the information to be carried in both the amplitude and phase or in different states of the polarisation of the optical field. Additionally, the selectivity of coherent receiver is very well suited for access networks. We present a 90° optical hybrid built on a silicon-on-insulator planar lightwave circuit, which can be used as the optical front end of the digital coherent receiver in a digitised RoF link and will lead to reduced receiver footprint and cost. The optical hybrid circuit includes 2×2 and 4×4 multimode interference (MMI) splitters, in a polarisation diversity configuration. The simulation results at vacuum wavelength 1,550 nm show polarisation independence and phase errors between the ports of less than 0.03°. The properties of the prototyped 4×4 MMI were measured over a wide range of wavelengths. The 2×2 and 4×4 MMI showed nearly equal splitting ratios. Measurements of the relative phase relationship between the ports for Transverse Electric mode polarisation are shown to match the simulation results.

Keywords Optical Hybrid · Silicon-on-insulator · Multimode interference couplers · Radio-over-fibre

S. Abdul-Majid (✉) · I. Hasan · Q. Zheng · R. Maldonado-Basilio · T. Hall
Centre for Research in Photonics, School of Electrical Engineering and Computer Science, University of Ottawa, 800 King Edward Avenue, Ottawa K1N 6N5, Ontario, Canada
e-mail: smajid@site.uottawa.ca

S. Bidnyk
Enablence Technologies Inc., 300 March Rd., Ottawa K1K 3H4, Ontario, Canada

1 Introduction

Radio-over-fibre (RoF) systems have attracted considerable interest because of their potential use in future broadband wireless communications. Generally speaking, radio-over-fibre technologies refer to the use of optical fibre links to distribute radio frequency (RF) signals from a central location to remote locations [1]. RoF technology finds its origins in fixed wireless local area networks that appeared in the late 1990s to provide wireless communication services in public places. Some years later, wireless networks have entered the home enabling wireless access to digital subscriber lines and cable access modems. The approach is appealing because the low loss and high bandwidth of the optical fibre network and the shorter range wireless terminations permit un-tethered and high-capacity connections.

For decades, RoF has been synonymous with analogue RF transport over an intensity-modulation direct-detection (IM-DD) optical fibre link; an approach that is plagued by nonlinearity and noise problems. More recently, architectures that break this mould to overcome these issues have been proposed and demonstrated. In one proposal [2], the analogue RF input signal is first digitised by an analogue-to-digital convertor and the data are then sent over a binary-shift-keyed IM-DD digital link and reconstructed by a digital-to-analogue convertor at the output. Despite the complexity, there are indications that digitised RoF might offer lower energy consumption primarily because a more sensitive photo-receiver may be used in the digital case [3]. In another proposal [4], analogue transport is retained but phase modulation is used to exploit the inherent linearity of phase modulators that make use of the electro-optic effect. The use of phase modulation necessarily requires the use of coherent detection. Once the use of coherent detection in RoF is embraced, it is a small step to consider the use

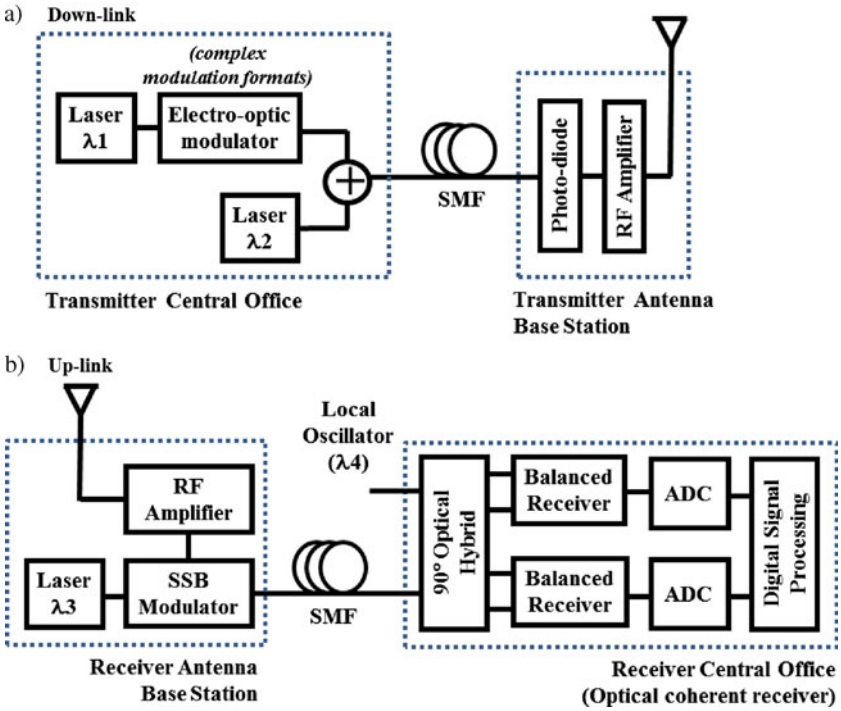

Fig. 1 Block diagram for the generation and detection of millimetre-wave carrier frequency signals using baseband RF and optical reception using SSB modulation combined with digital coherent optical detection. Note the presence of a 90° optical hybrid within the digital coherent receiver

of modern digitally enabled coherent optical transmission [5]. Today, RF baseband signals are generated digitally. One therefore has the option to transport the digital RF in native format end-to-end. The combined optical–wireless–optical channel is then a linear composition of the linear optical and wireless channels which is advantageous in simplifying the digital signal processing task of the RF hardware. Figure 1 provides a schematic of a digital coherent RoF link. The attention of the reader is drawn to the 90° optical hybrid at the heart of the receiver in the central office.

2 SOI based coherent receiver front end

As shown in Fig. 2a, an optical 90° hybrid is a six-port device (with two inputs and four outputs) used for coherent signal demodulation in fibre optic communications systems. Figure 2b provides a schematic design of the coherent signal demodulation system. The signal is split into its Transverse Electric (TE) and Transverse Magnetic (TM) polarised components, the components are rotated to align with the state of polarisation of the local oscillator (LO), and then passed to port #3 of the lower 4×4 multimode interference (MMI) and #1 of the upper 4×4 MMI. The LO is split by the 2×2 MMI, and its output signals are passed to #1 of the lower 4×4 MMI and port #3 of the upper 4×4 MMI. The output ports of the 4×4 MMIs provides four linear combination of the signal with the reference which differ by a relative phase shift between the signal and the reference of 0°, 90°, 180° and 270° thus providing the in-phase (I) and quadrature (Q) channels and their complements for both the TE and TM components of the signal.

Figure 3 shows the geometry of our designed 2×2 MMI. The ridge height h is equal to the thickness of the upper silicon layer throughout the device for simplicity. The geometry of the access waveguides is then defined by the ridge width W_A, and the centre-to-centre spacing L_1, between both input waveguides.

The spacing must be sufficient to render negligible the coupling between the access waveguides. The ridge width

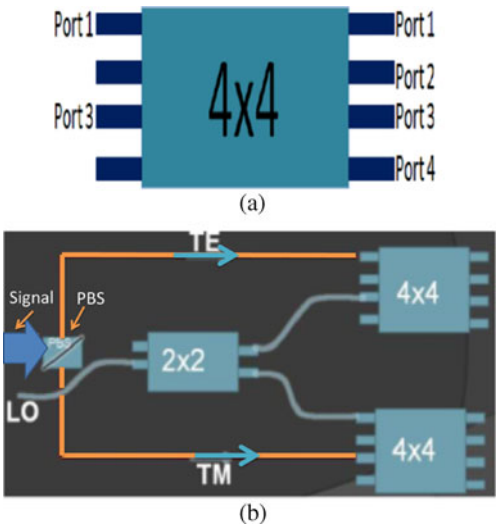

Fig. 2 **a** Schematic of the port configuration used to obtain a 90° hybrid using 4×4 MMI coupler. **b** Schematic design of the coherent optical receiver using 2×2 and 4×4 MMI couplers

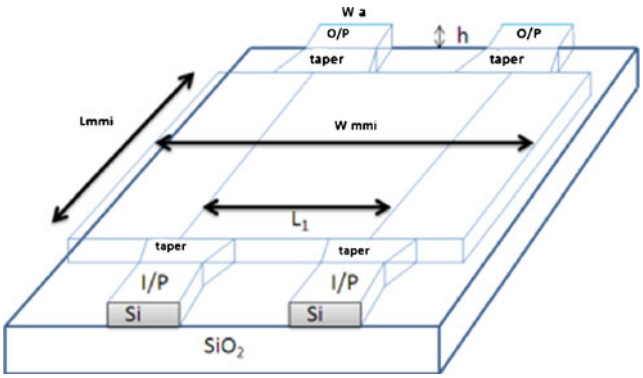

Fig. 3 Geometry of the 2×2 MMI [6]

of the access waveguides is chosen to control the number of guided modes. Ideally, the access waveguides are monomode, but they may support more transverse modes if care is taken to ensure only the fundamental mode is excited. The key components of the coherent detector circuit, including the 2×2 MMI, 4×4 MMI and polarisation diversity configuration have been designed and simulated, using the numerical mode solving tool FIMMWAVE from Photon Design. The 2×2 and 4×4 MMI have an overall length of 701 and 3,712.5 μm respectively. Tapers are used to couple adiabatically single mode waveguides to the entrance and exit ports of the MMI to assure correct operation by avoiding coupling to the higher order transverse modes allowed at the entrance and exit ports of the MMI.

The detailed design procedure, design parameters and the results of simulations were published in reference [6]. At the designed operating vacuum wavelength of 1,550 nm, the MMIs showed polarisation independence, phase errors between the ports of less than 0.03° and the smaller footprint that is achievable with a silicon-on-insulator (SOI) planar light-wave circuit (PLC) compared to an equivalent InP PLC.

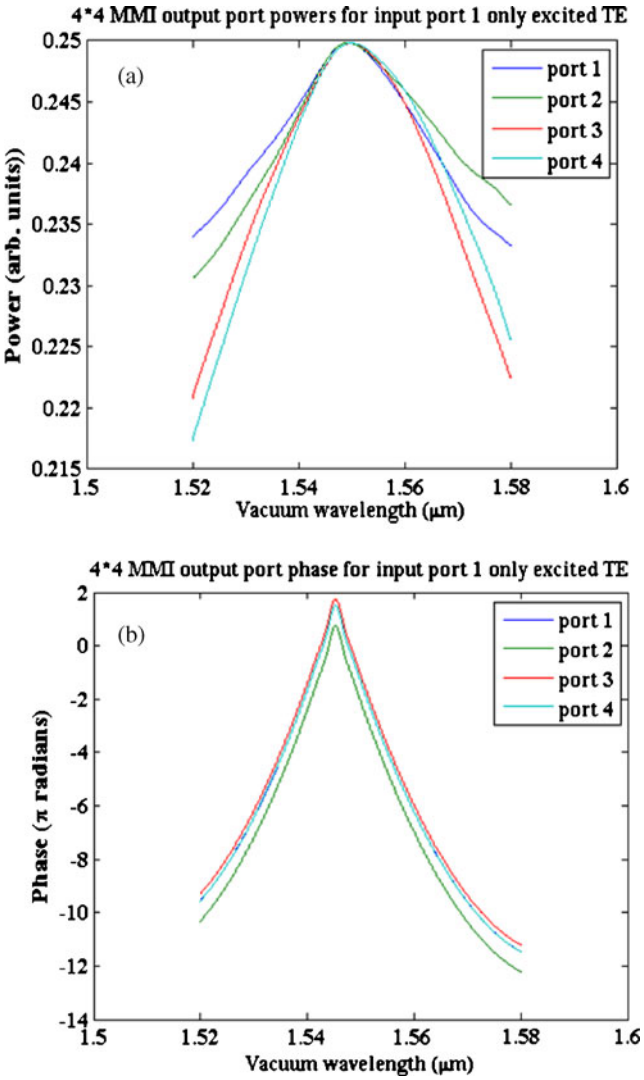

Fig. 4 4×4 MMI output port power and phase for TE polarised light injected into input port #1 only. **a** Optical power as a function of vacuum wavelength at each output port expressed as a fraction of the power injected into input port #1. **b** Unwrapped phase a function of vacuum wavelength at each output port expressed as a fraction of the power injected into input port #1. For this configuration, the phase response recorded at port #1 is identical to and has been overwritten by the phase recorded at port #4

3 Simulation results

A simulation using the FIMMWAVE tool from Photon Design enhanced by custom MATLAB code were used to simulate the behaviour of the 4×4 MMI over a 60 nm wavelength range between 1520 and 1580 nm .The simulation results for the 4×4 MMI are shown in Figs. 4, 5 and 6. The results for the TM case were essentially identical. The power and the phase of the light at all output ports were recorded as the wavelength was scanned for light injected into input port #1 only (Fig. 4) and input port #3 only (Fig. 5). The phase at an output port of the light from input #1 relative to the light from input port #3 derived from these results is shown in Fig. 6. It may be observed that the splitting ratios are almost equal and flat (to within ∼ 2%) over a wide bandwidth (∼20 nm) around 1550 nm. The port phase relations are in substantial agreement with theoretical predictions [7] (port #1: $\pi/4$; port #2: $-5\pi/4$; port #3: $-\pi/4$; port #4: $-3\pi/4$) at the designed operating vacuum wavelength of 1550 nm and are flat over the entire 60-nm range despite the significant decrease in magnitude and uniformity of the power splitting ratio at the extremes of the wavelength range. Choosing port #1 as the in-phase channel (I) then port #3 is the quadrature channel (Q); port #2 is the complement of the quadrature channel ($\overline{I}$); and port #4 is the complement of the in-phase channel ($\overline{Q}$).

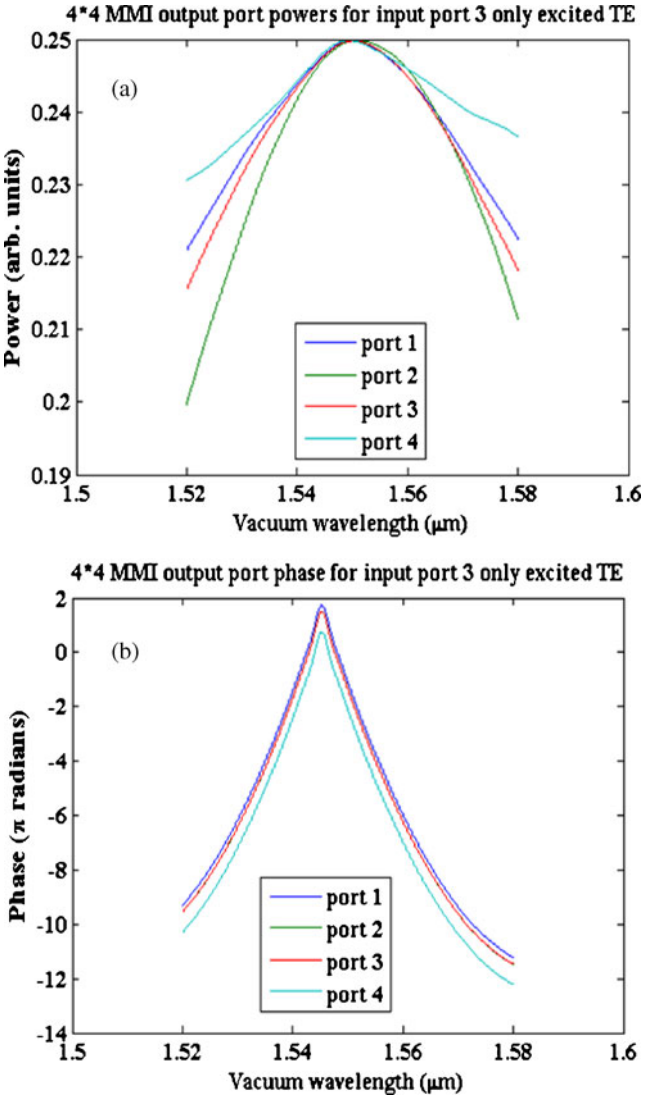

Fig. 5 4×4 MMI output port power and phase for TE polarised light injected into input port #3 only. **a** Optical power as a function of vacuum wavelength at each output port expressed as a fraction of the power injected into input port #3. **b** Unwrapped phase a function of vacuum wavelength at each output port expressed as a fraction of the power injected into input port #3. For this configuration, the phase response recorded at port 2 is identical to, and has been overwritten by, the phase recorded at port 3

When light derived from the same source is present at both input #1 and input port #3, interference will take place in accordance to the phase difference between the light at the two input ports and the relative phase relations between the ports intrinsic to the MMI. If the phase difference at the two input ports derives from an optical path-length difference, then the phase difference at the input ports will be proportional to frequency. The intensity of the light at each port as the frequency is scanned will therefore display fringes. Moreover, these fringes are phase-shifted with

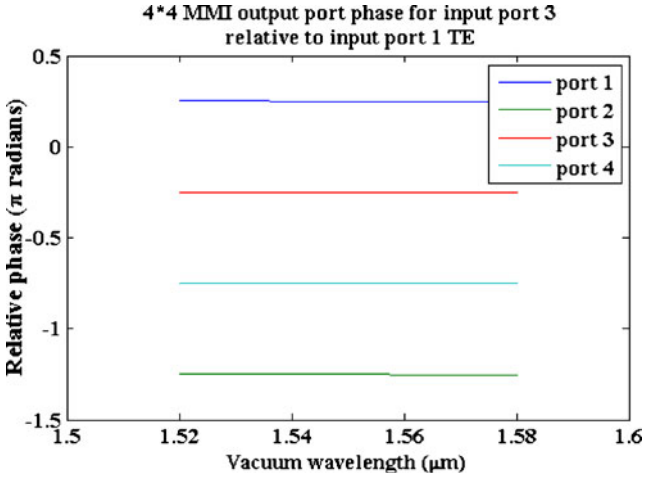

Fig. 6 The phase as a function of wavelength at each output port of light from input port #1 relative to the light from port #3

respect to each other in accordance to the intrinsic relative phase relations between the ports. This forms the basis of a method to experimentally measure the port relative phase relations. An analytic signal may be extracted from experimentally measured spectral interferograms using a Hilbert transform. The relative phase of the analytic signals between ports then yields the spectral distribution of the relative phase relations of the ports. An example of a simulated transmission spectrum used to verify the measurement technique is shown in Fig. 8b.

4 Test Results

4.1 Power splitting uniformity and polarisation independence

A PLC containing the 2×2 MMI, 4×4 MMI and polarisation beam splitters was fabricated at the Canadian Photonics Fabrication Centre with the support of CMC Microsystems. The wafers were cleaved at the Institut National d'Optique using the laser-assisted cleaving process they have developed. After microscopic inspection, the devices with the best waveguide facets were chosen to perform tests.

Table 1 Measured output powers for 2×2 MMI for both TE and TM polarised constant power light at the input port #1 or input port #2 at a vacuum wavelength of 1550 nm

WG #2	Output power (mW)		WG #2	Output power (mW)	
TE	O/P #1	O/P #2	TM	O/P #1	O/P #2
I/P #1	0.13	0.11	I/P # 1	0.13	0.13
I/P #2	0.12	0.13	I/P # 2	0.12	0.12

Table 2 Measured output powers for 4×4 MMI for both TE and TM polarised light at the input port #1 or input port #3 at a vacuum wavelength of 1550 nm

WG #5	Output power (mW)			
TE	O/P #1	O/P #2	O/P #3	O/P #4
I/P #1	0.095	0.070	0.070	0.087
I/P #3	0.093	0.070	0.080	0.010
TM				
I/P # 1	0.089	0.076	0.073	0.090
I/P # 3	0.096	0.071	0.082	0.080

Polarisation-independent operation and robustness to tolerances were considered at the design and simulation stages. To verify that our designed MMIs can handle both TE and TM modes equally well, tests of equal splitting ratio and polarisation independence were first conducted. Both 2×2 MMI (WG #2) and 4×4 MMI (WG #5) were tested experimentally. The test was performed using a PLC probe station using a pair of Newport three-axis alignment stages.

First TE polarised light was injected into input port #1 of 2×2 MMI, and the optical power from each output port was measured. The polarisation was then rotated to TM, and the measurements were repeated. The same test was repeated for polarised light injected into input port #2. The uniformity of the splitting ratio for the 4×4 MMI inputs has been tested also with TE and TM polarised light injected into first input port #1 and subsequently separately into port #3. The results of these measurements are organised in Tables 1 and 2. The results demonstrate that the 2×2 and 4×4 MMIs can handle TE and TM polarised inputs equally well.

4.2 Measurement of the relative phase relationships between ports

In this section, we report experimental results demonstrating the broadband quadrature phase behaviour of the compact SOI 4×4 MMI couplers that are realised in SOI rib waveguide. The measurement results verify the potential application of SOI-waveguide-based optical 90° hybrid in a coherent optical receiver. To evaluate the phase behaviour of 4×4 MMI couplers, we constructed a 4×4 delayed interferometer based on the MMI coupler, as shown in Fig. 7. Only input ports #1 and #3 of the 4×4 MMI coupler are used. A customised holder is used to hold a fibre matrix to enable simultaneous excitation of the two ports. The path-length difference of the two input fibres to ports #1 and #3 is adjusted so that the interferometer has a free-spectral range (FSR) of 0.52 nm. The data analysis method does not need to know the precise path-length difference.

The measurement is implemented by sweeping the wavelength of the input optical signal with a step of 0.02 nm and monitoring the transmitted optical power at each output port during sufficient dwell period for the tune-able laser to settle. A PC running a LabView programme controls the tuneable laser and acquires the data from the photo-detector to perform the measurement in a fast and accurate manner. Figure 8a shows a typical measured TE transmission spectrum at a port of the fabricated 4×4 MMI employing the experimental arrangement and apparatus illustrated in Fig. 7.

Sinusoidal fringes are observed within an envelope over a 20-nm bandwidth (1,540–1,560 nm). The zoom-in view of the interference fringe verifies an FSR of 0.52 nm. The envelope varies more wildly than expected when compared to the simulated spectra shown illustrated by Fig. 8b. Although the FSR of the fringes differs in this example, that does not alter the envelope which is determined by the slow variations with wavelength in the splitting ratio spectra in a completely stable setup.

Differences in launched power and/or polarisation state lead to a reduction in the fringe contrast. The observed variations in fringe magnitude and average are therefore most likely the result of the launch conditions varying during the period of time (many minutes) taken by the wavelength scan due to environmental perturbations

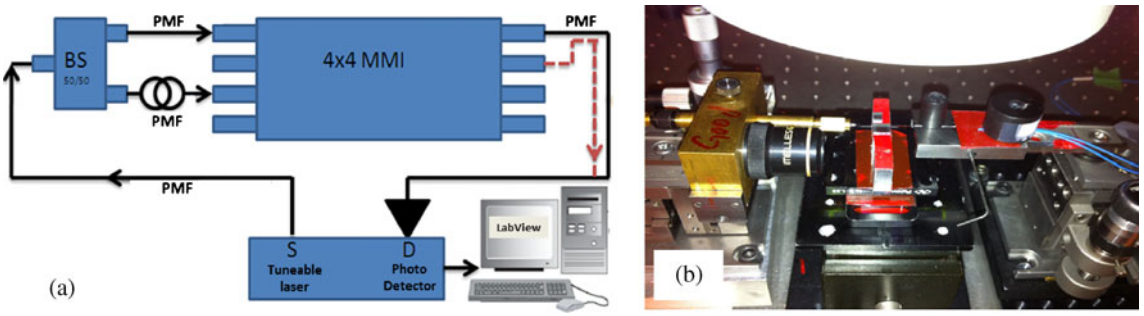

Fig. 7 Experimental arrangement to test a 4×4 MMI based on an imbalanced interferometer. **a** Schematic of the interofermetric arrangement. **b** Photograph of the customised fibre optical launch jig mounted upon three-axis alignment stages

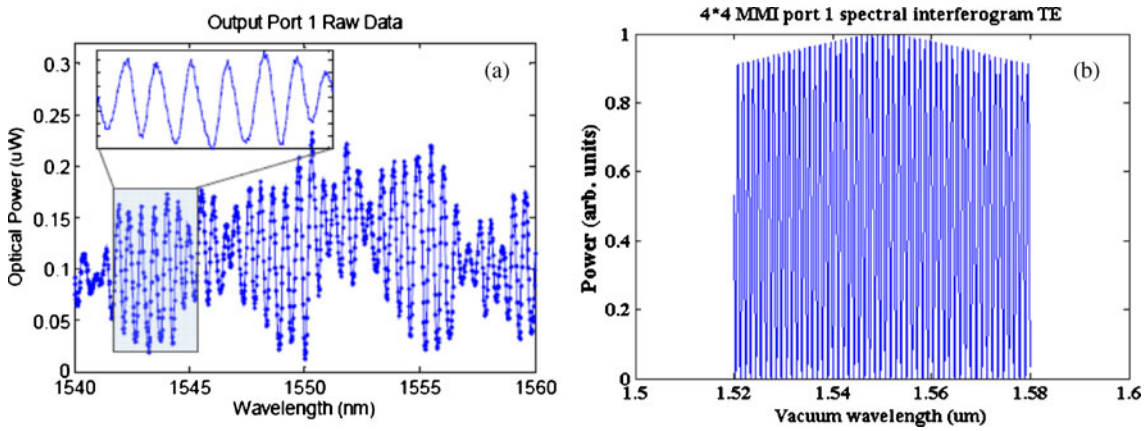

Fig. 8 Comparision of measured and simulated transmission spectra for output port 1. The spectra for the remaining ports are similar. **a** Measured transmission spectra for output port #1. **b** Simulated transmission spectra for output #1 and an optical path length difference from source to input port of ∼2.4 mm

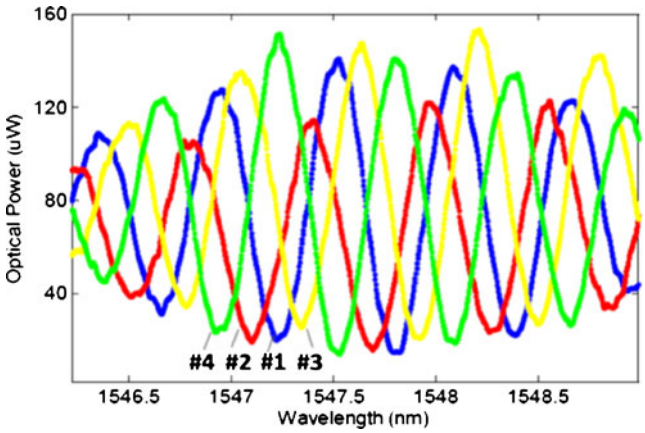

Fig. 9 Spectral interferogram measured at all the output ports. Labels indicate the respective output port

(e.g., vibration) to the apparatus. The integration of the interferometers beam splitter, input optical waveguides, delay and the 4×4 MMI device on the same chip will eliminate these perturbations greatly improve the measurement accuracy.

Scans over a narrower wavelength range take less time and were found to be more stable as a result. Figure 9 shows that the interference fringes at all the output ports are measured over a 3-vacuum wavelength range. The labels indicate the respective output port. It can be seen that spectral shifts of a quarter of the FSR are observed, indicating the desired $\pi/2$ phase shifts between the output ports. The phase information of spectral interference fringe at each

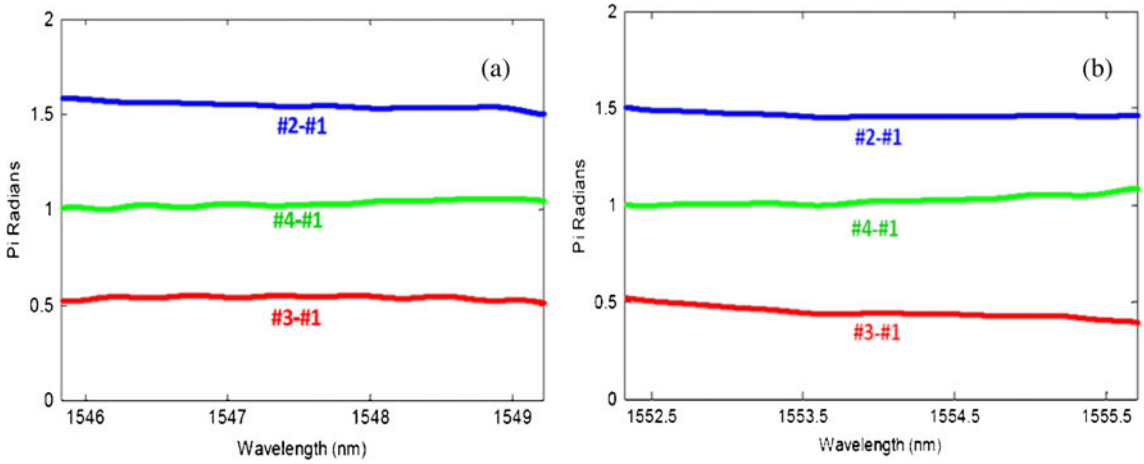

Fig. 10 Output port relative phase relations extracted from transmission spectral data. **a** Measured relative phases at the output ports with respect to port #1 over a 3 nm bandwidth (from 1546 to 1549 nm). **b** Measured relative phases at the output ports with respect to port #1 over a 3 nm bandwidth (from 1552.5 to 1555.5 nm)

output port is extracted using a digital Hilbert transform. The results are plotted in Fig. 10 for two disjoint 3-nm wide wavelength ranges and show a flat wavelength dependence of the relative phases close to the target values, verifying the predictions of simulations.

5 Conclusions

A compact SOI-based 4×4 MMI coupler was designed, fabricated and tested with an emphasis on phase performance. Quadrature optical phase behaviour was observed over a 20-nm wide spectral range around 1550 nm, verifying its functionality as a 90° optical hybrid for application to digital coherent optical receivers that feature in novel coherent optical RoF architectures.

Acknowledgements This work was supported by the Natural Sciences and Engineering Research Council Canada, CMC Microsystems and Enablence Ltd. The PLC hybrids were fabricated at the Canadian Photonics Fabrication Centre. Dr Hall is grateful for the support of the Canada Research Chairs Program.

References

1. Lim C, Nirmalathas A, Bakaul M, Gamage P, Lee K-L, Yang Y, Novak D, Waterhouse R (2010) Fiber-wireless networks and subsystem technologies. J Lightwave Technol 28(4):390–404
2. Yang Y, Lim C, Nirmalathas A (2010) Multichannel digitized RF-over-fiber transmission based on bandpass sampling and FPGA. IEEE Trans Microwave Theor Tech 58(11):3181–3188
3. Yang Y, Lim C, Nirmalathas A (2011) Comparison of energy consumption of integrated optical-wireless access networks, optical fibre communications (OFC 2011), JWA82
4. Clark TR, Dennis ML (2007) Coherent optical phase-modulation link. IEEE Photonics Technol Lett 19(16):1206–1208
5. Caballero A, Zibar D, Sambaraju R, Mart J, Monroy I. T. (2012) High-capacity 60 GHz and 75110 GHz band links employing all-optical OFDM generation and digital coherent detection. J Lightwave Technol 30(1):147–155
6. Abdul-Majid S, Hasan II, Bock PJ, Hall TJ (2010) Design, simulation and fabrication of a 90° SOI optical hybrid based on the self-imaging principle, photonics Europe, conference on silicon photonics and photonic integrated circuits II, Brussels, Belgium, 12–16 April 2010, SPIE 7719, 2010, art. 77190E
7. Nikkhah H, Zheng Q, Hassan I, Abdul-Majid S, Hall TJ (2012) The free space and waveguide Talbot effect: phase relations and planar light circuit applications. Photonics North 2012, Montreal, Canada, June 2012, Proc. SPIE 8412, art. 841217